Possible fates of the dispersion of SARS-COV-2 in the Mexican context

I. Santamaría-Holek[1], V. Castaño[2],

[1] *UMDI-J, Facultad de Ciencias, Universidad Nacional Autónoma de México, Juriquilla, Querétaro, CP 76230, México and*

[2] *Centro de Física Aplicada y Tecnología Avanzada, Universidad Nacional Autónoma de México, Juriquilla, Querétaro, CP 76230, México*

Abstract

The determination of the adequate time for house confinement and when social distancing restrictions should end are now two of the main challenges that any country has to face in an effective battle against. The possibility of a new outbreak of the pandemic and how to avoid it is, nowadays, one of the primary objectives of epidemiological research. In this work, we go deep in this subject by presenting an innovative compartmental model, that explicitly introduces the number of active cases, and employing it as a conceptual tool to explore the possible fates of the dispersion of SARS-COV-2 in the Mexican context. We incorporated the impact of starting, inattention, and end of restrictive social policies on the time evolution of the pandemics via time-in-run corrections to the infection rates. The magnitude and impact on the epidemic due to post-social restrictive policies are also studied. The scenarios generated by the model can help authorities to determine an adequate time and population load that may be allowed to reassume normal activities.

I. INTRODUCTION

Humankind and environment are bidirectionally linked through a dynamical hierarchical feedback [1–6]. Society impacts the natural systems by exploiting, extracting, and (sometimes) restoring resources, as well as polluting. The environment affects social networks by providing or restricting the resources required for their survival [7]. If the relation between both systems implies that their impacts do not threaten their existence, the relationship is sustainable [6, 8].

Mankind and environment are bidirectionally linked through a dynamical hierarchical feedback [30–35]. The society impacts the natural systems by exploiting, extracting and (sometimes) restoring resources, as well as polluting and leaving waste. The environment impacts the social systems by providing or restricting the necessary resources for their survival [36]. If the relation between both systems implies that their impacts does not threat their existence in the future, the relation is sustainable [35, 37].

Overpopulation, overconsumption, and economic inequality have decreased the stablity of social-ecological systems. This fact leads to possible unsustainable future scenarios and risks the viability of the roles and functions of both human and natural systems [3–5].

The actual SARS-COV-2 pandemic is an excellent example of how a natural event can break this coupling among societies and the environment. Historically, many civilizations have collapsed due to their inadequate resource-management policies and the lack of an ability to modify their cultural practices, like the consumption of non-traditional foods [9, 10], thereby creating unsustainable trajectories [5]. The beginnings of pandemics often result from the transgression of animal habitats and leads to severe disruption and damage to our lives in both the public health and economic domains [6, 11, 12].

Given the global character of SARS-COV-2, innovative epidemiological analyses are required, which could include complex network analysis and conceptual maps for the entire system [13]. Additionally, compartmental epidemiological models can address the spread of disease by classifying sectors of the total population, and analyzing how each sector interacts with another sector. An example of these models is the classical SIR and SEIR models (susceptible, exposed, infected, and recovered individuals), among others [14, 15]. The importance of these models is clear since they allow us to determine the time evolution of the pandemics based on clinical aspects of the disease [15, 16]. They are very important

in virology and in epidemiology to control outbreaks, invasions and transmissions[10, 17–20], and also for informing and analyzing health policies[13, 19, 21, 22]. Several models of the spread and dynamics of the SARS-COV-2 epidemic have recently been proposed [23], but works with the prospectives approach presented in the article are not available, to our knowledge.

This work aims to evaluate the duration and effects of the health policies implemented on the different sectors and the effect of the time dependence of the social distancing and house confinement measures. Our modeling strategy allows us to reach this objective and has some similitudes with SEIR and SEID models and shares some aspects with a recent model proposed in Ref. [15]. Innovations come from the type of interaction among sectors and the introduction of time dependent modifications of the infection constants that allow us to accurately account for the effect of social distancing and house confinement measures and the pressure due to the inattention of the economy on those measures. Informative campaigns are helpful but find resistances related to the very heterogeneous cultural, social, and epistemological characteristics of the Mexican population.

II. THE MODELING MECHANISM AND THE EVOLUTION EQUATIONS

An essential aspect of the dispersion of SARS-COV-2 in the population is the relatively large incubation time of the virus and their differential symptoms among different sectors of the society allowing asymptomatic individuals to infect vulnerable sectors without either of them noticing initially. In this sense, high hygiene standards, as well as social distancing, are the measures recommended to stop the spread of the disease.

In this work, we will use a variation of the known SIER and SIRD compartmental models of epidemiology. The variations introduced are essential to account for the importance of social distancing and house confinement recommendations in the time evolution of the epidemic. Our introduced modifications of these models also contribute to a better understanding of the resulting future scenarios depending on governmental decisions as to the duration of the social distancing and domestic confinement, as well as the utility of restrictions imposed on society after ending lock-down. This model considers the specific characteristics of the dispersion of the SARS-CoV-2 virus among humans. The parameters of the model are estimated according to clinical observations reported in the literature.

Additionally, information available for the Mexican case to the date of May 19, is used.

We consider that there are three different ways of a susceptible individual (S) of being infected: by direct physical contact with the virus (V) through, for example, contaminated surfaces in public transport; contact with an individual exposed to the virus (E), and by contact with someone infected (I). The difference between infected and exposed individuals is related to the severity of the symptoms of the individual. In the former sector are notorious, while in the latter, the symptoms are mild or non-existent. This drastic contrast is, in part, the cause of an important under-registration of the total number of infected individuals. These *contacts* can be modeled by the reactions:

$$S + V \xrightarrow{\mathrm{k}_v} E, \tag{1}$$

$$S + E \xrightarrow{\mathrm{k}_e} 2E, \tag{2}$$

$$S + I \xrightarrow{\mathrm{k}_i} E + I. \tag{3}$$

Coefficients k_j with $j = V, E, I$ is proportional to the probability of encountering a susceptible member S with a member of the j group. The three contagion mechanisms suppose that the result is always an exposed member with no initial symptoms that after three to nine days start presenting symptoms.

Importantly, these rate constants are time-dependent functions since they change during and after the quarantine time in a way that we approximate as

$$k_j^0(t) = k_j - \Delta k_j^{di}\theta(t - t_i) + \Delta k_j^{ep}\theta(t - t_e p) + \Delta k_j^{f}\theta(t - t_f), \tag{4}$$

where k_j is the infection rate and $\theta(t - t_k)$ (with $j = i, ep$) is the Heaviside step function centered at the initial time of the domestic confinement t_i and social distancing measures $[\theta(t-t_i)]$. This term is negative because these measures decrease the infection rate. The third term at the right-hand side is positive since it represents the increase of the infection rate due to economic inattention, which takes place at $t_e p$ $[\theta(t - t_{ep})]$. The last term corresponds to the contagion rate's increase due to the ending lock-down, which takes place at t_f. The parameters Δk_j^{di}, Δk_j^{ep} and Δk_j^{f} measure the fall and rise of each contact rate due to the start of the house confinement, its inattention, and the end of the confinement measures.

Once the virus is present in an exposed member, he/she can develop symptoms or recover by himself/herself. Therefore, we will consider that the evolution of the exposed individuals

occurs according to

$$q\,E \xrightarrow{\alpha} I, \tag{5}$$

$$(1-q)\,E \xrightarrow{\beta} R, \tag{6}$$

respectively. In these reactions, we have introduced the statistical parameter q that measures the proportion of exposed individuals, E, that goes on to manifest symptoms ; $1-q$ is, therefore, the fraction of exposed individuals that eventually recover. We assume that it is improbable that an infected individual with no symptoms could die.

In reactions (2.5) and (2.6), the inverse of α and β measure the characteristic times of each process: α^{-1} is the time of an exposed individual to start presenting symptoms (between 3 and 9 days with median ≈ 6 days), and β^{-1} is the time of recovery for mild cases (between 14-21 days) [24–26]. The lack of data on the number of exposed individuals that do not develop symptoms and recover compels one to fit the official data by assuming that $q \simeq 1$, which implies that Eq. (2.6) is vanishingly small. This drastic assumption is necessary for avoiding speculations on the number of exposed individuals and can be avoided in turn if disease tests are extensively applied to the population.

At a given time t, the sector of infected individuals developing symptoms consists of three subsectors with different proportions that could be statistically measured. However, they are not explicit in the data reported by authorities.

Two of these three subpopulations correspond to the portion of individuals that recover and die. The third one is, by definition, the number of active individuals (A), that is, those that are infected but are still not recovered or dead. This dynamics can be represented by

$$r\,I \xrightarrow{\gamma} R, \tag{7}$$

$$d\,I \xrightarrow{\delta} D, \tag{8}$$

$$a\,I \xrightarrow{\epsilon} A, \tag{9}$$

where statistical information enters through the parameters r, d, a, which measures the proportion of individuals that recover, die or are active from the total number of known infected individuals, and satisfy the condition $r+d+a=1$. Mathematically, it is equivalent to avoid these parameters and only change appropriately the rate constants during the fit of the data. However, we have introduced them to not change the stoichiometryof the population I. The

population I naturally subdivide into three sectors, A; R and D, each one statistically measurable. These parameters depend on thepublic health status of each country and on the quality of the healthcare. The rate at which the individuals pass from one state to another is related with the intrinsic interaction of a single individual with the virus.

The parameter γ^{-1} measures the characteristic time of recovery from a seriously ill individual, meaning that who requires hospitalization (between 14 and 21 days), and δ^{-1} is the characteristic time endured from the beginning of symptoms until death (which ranges between 17 and 21 days) [24–26]. The parameter ϵ is the period during which an infected individual maintains manifests active symptoms, and thus it will be considered similar to α. This assumption is validated, *a posteriori*, by the fact that five fits are performed simultaneously. These are the total number of individuals of infected, recovered, dead sectors together with the number of active and of daily cases. Notice that the parameters α, β, γ, δ, and ϵ depend mainly on features of the virus in humans and not on social contact or hygiene.

Eq. (2.9) introduces an additional delay in the evolution of the epidemic. The final steps of the evolution are determined by

$$p\,A \xrightarrow{\delta} D, \tag{10}$$

$$(1-p)\,A \xrightarrow{\gamma} R, \tag{11}$$

since an active individual only can recover or die. In these last relations, we have assumed that the recovering and death rate constants are the same as in the case of the infected sector. This assumption can be relaxed accordingly with the characteristics of the data compiled for the disease. We have also introduced the statistical parameter p which, as mentioned before, could depend on the quality of the healthcare. In Mexico, according to the official reports, this proportion ranges from 9% to 12% of the known infected population [27]. Therefore, the parameter will take values in the range $p \approx 0.09 - 0.12$.

Using the previous relationships, the non-linear dynamics of the different sectors becomes:

$$\frac{dS}{dt} = \mu S - (k_v V + k_e E + k_i I)S, \tag{12}$$

$$\frac{dE}{dt} = (k_v V + k_e E + k_i I)S - [q\,\alpha + (1-q)\,\beta]E, \tag{13}$$

$$\frac{dI}{dt} = \alpha\, q\, E - (\gamma\, r + \delta\, d + \epsilon\, a)I, \tag{14}$$

$$\frac{dA}{dt} = \epsilon\, a\, I - [\delta\, p + \gamma(1-p)]A, \tag{15}$$

$$\frac{dR}{dt} = \gamma\, r\, I + \beta\,(1-q)\,E + \gamma\,(1-p)\,A, \tag{16}$$

$$\frac{dD}{dt} = \delta d\, I + \delta p\, A. \tag{17}$$

In this mechanism, the total count of all members of all groups $N = S + E + I + A + R + D$ obeys $dN/dt = \mu S$, where μ is the exponential growth constant (rate of births minus deaths) of Mexican population before the entrance of the virus. Since we are interested only in the effects of the pandemic event we will assume without loss of generality that $N(t) = N_0$ is constant ($\mu = 0$).

The number of individuals susceptible to be infected can be estimated after recognizing that approximately 75-78% of the population is urban (cities having 2.5 thousand individuals or more) [28]. Hence, the total number of urban populations is about 101.4 million. From this urban population, 0.3% may be infected, according to statistical data. That is, the number of susceptible individuals can be estimated at around $S_0 \approx 305$ thousand individuals. If the rural population included, then the statistical estimation is about 400 thousand individuals.

III. RESULTS

The data reported by the authorities are: *i*) the (cumulative) number of confirmed cases, *ii*) the number of recovered individuals, *iii*) the number of deaths, *iv*) the number of active cases and *v*) the number of new infections per day. There is a lack of measured information about exposed individuals since the Mexican authorities did not apply extensive COVID-testing for detection. Because of this, the total number of infected individuals cannot be fitted directly, due to the lack of information about the exposed population $E(t)$. However, this situation is avoided in our model because we are explicitly incorporating the number of active cases. Thus, the infected population has three options to evolve: to recover, to die, or to be active according to the statistical proportions, as previously discussed.

A. Fit criteria

To be reliable, the fit of data for the total number of confirmed infected individuals, Confirmed(t), has to be simultaneous with the fit of the number of recovered and dead individuals, as well as with the daily number of infected individuals, Day(t), and the number of active cases, $A(t)$. That is, for reliable predictions from the model, these five fits have to be performed simultaneously.

The total number Confirmed(t) of confirmed infected individuals as a function of time is given by the sum of the three sectors entering into relations (2.7)-(2.9), that is

$$\text{Confirmed}(t) = R(t) + D(t) + A(t), \tag{18}$$

which is obtained by a simple conservation of individuals.

The number of daily infected individuals is proportional to the cumulative number of infected individuals multiplied by the inverse characteristic times of those becoming active, recovered or death see Eq. (2.14), that is

$$\text{Day}(t) = (\gamma\, r + \delta\, g + \epsilon\, a) \int_1^t \left[I(t') - I(t'-1) \right] dt', \tag{19}$$

which is the loss term of Eq. (2.14).

B. Results

The set of Eqs. (2.12)-(2.17), together with the definitions (3.1) and (3.2), were used to fit the data reported by the Mexican authorities on the number of confirmed cases (red circles), recovered (blue squares), and deaths (orange triangles) in figure 1a), see Ref. [29] for deatils. Simultaneously, we used definitions (3.1) and (3.2) together with the reported data to obtain the number of active cases and the daily number of infected individuals, figure 1c). In figure 1a) and b), the lines are the fits of our model for the Confirmed (black), Recovered (blue), Death (orange), Infected (red), Exposed (magenta) and Active (cyan) sectors. Figure 1b) shows the long term projection of the model after assuming that the number of susceptible individuals was about 61% of the initially estimated number ($S_0 = 187$ thousand). Simultaneously, we have make fits of figures 1c) and d), that report the number of active cases (blue dashed line) and the number of daily cases (black line). No fit of the

number of exposed individuals $E(t)$ (magenta) is possible since no extensive testing has been applied to the Mexican population.

The maximum of the infection curve takes place around the days 75-85, corresponding to days between May 12 to 22. The projection suggests that the 97% point of the pandemic is reached (with the actual social distancing and house confinement infection rates) about the week of November 1 to 7 (days 246-252). The number of new daily cases and active cases have their maxima about days 80 (May 19) and 125 (July 3), respectively.

The estimation of the infection rates for exposed k_e and infected k_i sectors assumes that they have to be $10^2 - 10^3$ times the inverse of the Mexican population (7.7×10^{-9}), that is, they must lie in the range $10^{-7} - 10^{-6}$days^{-1} [15]. The rate at which symptoms appear is estimated to be in the interval of $10^{-2} - 10^{-1}$ days^{-1}, whereas the recovery rate β was assessed on the range 10^{-2}days^{-1}, both consistent with clinical observations [24–26].

The rate of k_v and the parameter V, the virulence, are the triggering ones and are a measure of the hygienic conditions, meaning that infections can occur not only through personal contact. The effective virulence factor k_vV has therefore a value in the range $10^{-6} - 10^{-5}$. This estimation is important to determine the initial slope of the curve of the cumulative number of cases. In our simulations they take the value $k_vV \approx 5.7 \times 10^{-3}$.

Figure 2a) shows details of the time evolution of the active and daily cumulative cases $A(t)$ and $Day(t)$, respectively, as a function of time and compared with the data reported. It is indicated the day at which the domestic confinement measures were initiated, day 23 (March 23), and the day at which many people ended confinement to their homes due to economic pressure, day 50 (April 19), leading to a weakening of those measures. These measures were accounted for by introducing the corrections explained in Eq. (2.4) into Eqs. (2.12) and (2.13):

$$\frac{dS}{dt} = \mu S - \left[k_vV + \tilde{k}_e(t)E + \tilde{k}_i(t)I\right] S, \tag{20}$$

$$\frac{dE}{dt} = \left[k_vV + \tilde{k}_e(t)E + \tilde{k}_i(t)I\right] S - (\alpha + \beta)E, \tag{21}$$

where

$$\tilde{k}_e(t) = k_e - \Delta k_e^{di}\theta(t - t_i) + \Delta k_e^{ep}\theta(t - t_{ep}), \tag{22}$$

and

$$\tilde{k}_i(t) = k_e - \Delta k_i^{di}\theta(t - t_i) + \Delta k_i^{ep}\theta(t - t_{ep}). \tag{23}$$

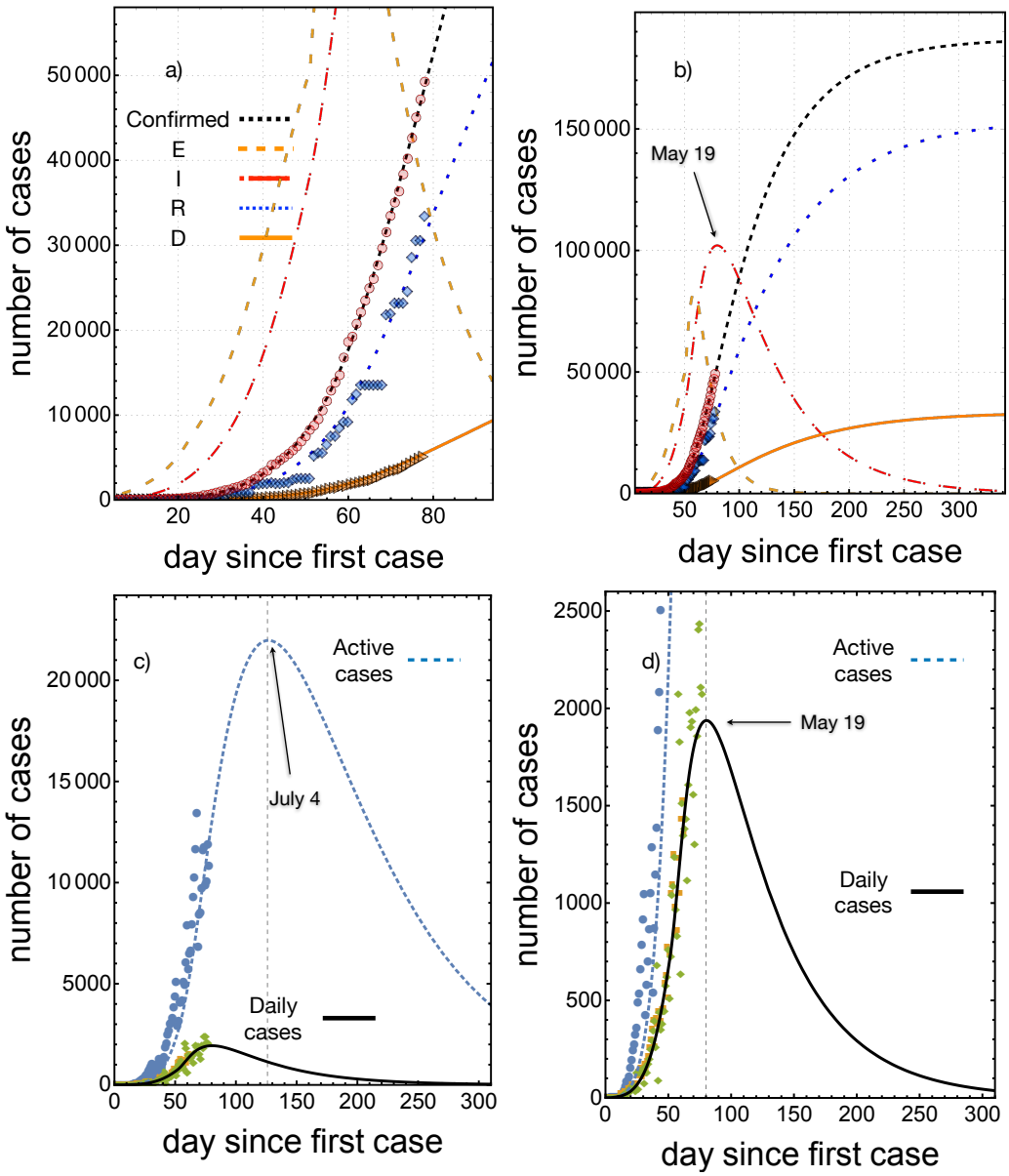

FIG. 1. Fit of the data reported by the Mexican authorities (up to May 19). a) The symbols represent infected (red circles), recovered (blue squares), and death (orange triangles) individuals, the lines the numerical solutions of Eqs. (2.12)-(2.17) for $I(t)$ (red), $R(t)$ (blue), $D(t)$ (orange), exposed $E(t)$ (magenta) and active $A(t)$ (cyan). The black dashed line is the number of confirmed cases given by Eq. (19). b) Long term projection of the fit. c) Fit of the active cases and d) of the cumulative number of daily cases $Day(t)$. The calculation of the data represented by the symbols was done using Eq. (3.2) (green diamonds squares) and Eq. (3.1) (blue circles). In the case of daily cases (orange squares), we also used data from Johns Hopkins COVID-19 global map to corroborate that our determination of the daily cases coincides with the data reported in Ref. [27].

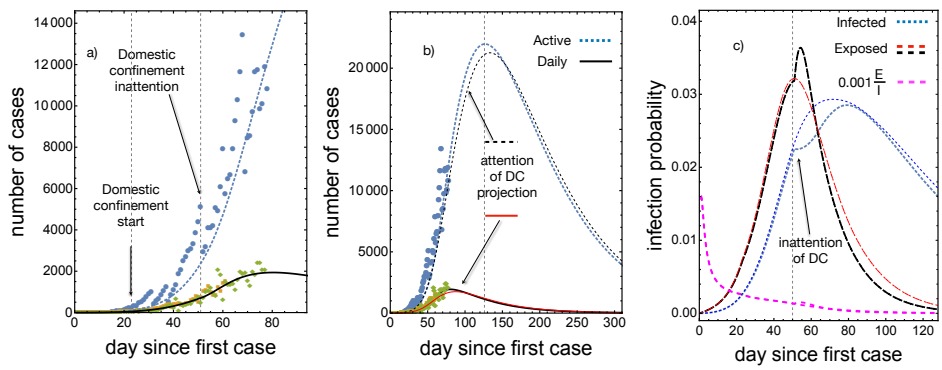

FIG. 2. Fit of the data for the active number of cases and daily cases reported by the Mexican authorities (up to May 19) [27]. a) The symbols represent infected (red circles), recovered (blue squares) and death (orange triangles) individuals, the lines the numerical solutions of Eqs. (2.12)-(2.17) for $I(t)$ (red), $R(t)$ (blue) and $D(t)$ (orange). It is also reported the prediction of the number of exposed individuals $E(t)$ (magenta). b) Prediction of the long term of the pandemic and of the final values of the populations considered. c) Infection probability rate as a function of time for the exposed and infected individuals.

The definitions of Δk_i^{di} and Δk_i^{ep} is given after Eq. (2.4).

The implementation of social distancing and domestic confinement lead, in the first stage, to a reduction of 11% of the infection rate of both infected and exposed individuals ($\Delta k_i^{di} = 7.15 \times 10^{-8} s^{-1}$). However, by April 19, circumstances associated with economic pressure (survival) produced a significant increase in the number of daily cases due to the rise in the infection rate of about 70%. This increase is evident when comparing with the case of the prediction with social distancing methods intact, see figure 2b), black dashed and solid black lines, from where it is clear that an increase of about 5% of the active and daily cases took place. The dashed blue and red lines are the predictions under the assumption that social distancing and domestic confinement were respected. The blue line corresponds to an increase of the infection rate of $\Delta k_i^{ep} \approx 4.6 \times 10^{-7} s^{-1}$. It entered into play in the time evolution of the model on April 19 (day 50). This small increase considerably improved the fit of the infection data in figure 1 and is responsible for the increase of the active and daily cases. The accuracy of the prediction in the last stage is because the reporting of the number of individuals recovered after day 51 has been more systematic.

The figure 2c) shows the time evolution of the infection probability rates which are defined

by

$$P_e = k_e \frac{E(t)}{S_0} S(t), \tag{24}$$

$$P_i = k_i \frac{I(t)}{S_0} S(t), \tag{25}$$

$$\tag{26}$$

where S_0 is the maximum number of susceptible individuals. The maximum of the infection probability rate of exposed and infected individuals takes place between days $47 - 52$ (April $16 - 21$) and on $60 - 65$ (April 29-May 4), respectively. Therefore, the overall maximum of the infection probability rate ranged between days of $47 - 65$. These two parameters are reasonable measures of the intensity of daily infection and are proposed on the basis that the zero-order approximation of the joint probability of infection between susceptible and exposed or infected individuals is proportional to the product of the probabilities of being susceptible and infected or exposed.

C. Domestic confinement and social distance end

The projection of the impact of domestic-confinement end on the evolution of the epidemic assumes that a certain amount of individuals returns to the public life and that they can be infected by two mechanisms: *i)* Poor hygienic conditions and *ii)* contact with an exposed individual. Here, we suppose that contact with infected individuals (those that show symptoms) is less due to the use of prescribed preventative medicines. From the number of individuals that return to its economic activity, one may estimate, in a similar form as in the previous section, that one-third of them become susceptible to infection and, therefore, trigger a pandemic outbreak.

This new community of individuals will have the same structure as the original one (S_2, I_2, A_2, R_2, D_2) and therefore will show a similar dynamics. However, the triggering contact interactions are modified since they should reflect the actual status of the pandemic, that is, the new community becomes infected because of the community already infected. This

may be represented by

$$S_2 + V \xrightarrow{\mathrm{k}_v} E_2, \tag{27}$$

$$S_2 + E \xrightarrow{\mathrm{k}_e} E_2. \tag{28}$$

$$S_2 + I \xrightarrow{\hat{k}_i} E_2, \tag{29}$$

where we will assume $\hat{k}_i \sim k_i/3$. The successive evolution is determined entirely similar as in the original case, that is, by the sequence of interactions

$$E_2 \xrightarrow{\alpha} I_2, \tag{30}$$

$$r\, I_2 \xrightarrow{\gamma} R_2, \tag{31}$$

$$d\, I \xrightarrow{\delta} D_2, \tag{32}$$

$$a\, I \xrightarrow{\epsilon} A_2, \tag{33}$$

$$p\, A_2 \xrightarrow{\delta} D_2, \tag{34}$$

$$(1-p)\, A_2 \xrightarrow{\gamma} R_2, \tag{35}$$

The differential equations corresponding to the last reactions are similar to the set previously considered, Eqs. (2.12)-(2.17), with the respective reaction rates. For this second community we have assumed no corrections to the rate constants equivalent to those in Eq. (2.4), but multiplied the left hand side of the evolution equations for S_2, E_2 and I_2 by the Heaviside step function $\theta(t - t_f)$ centered at the end of the house confinement measures t_f.

Figure 3 shows the consequences of changing the ending of house confinement time, according to the model proposed. The figures 3 a) and b) correspond to ending the domestic confinement at day 90 (May 29) for two new susceptible populations $8 \cdot 10^4$ and $16 \cdot 10^4$. The impact is relevant in all the populations considered. The more drastic effects are in the number of infected individuals that increase the pandemic's duration by about 30 days. Most important is that the peak of the number of active cases is shifted to day 150 and increased by about 23%. The figures 3 c) and d) correspond to finishing the domestic confinement at day 110 (July 4) for the same number of new susceptible populations. In this case, the duration of the pandemic increases for about 30 days. The peak of the number of active cases is shifted to day 160 but only increased by about 9%. Finally, it is worth noticing that if the original dynamics could be maintained even after the end of domestic confinement, the pandemic's period is about 300 days. If not, in the worst case considered

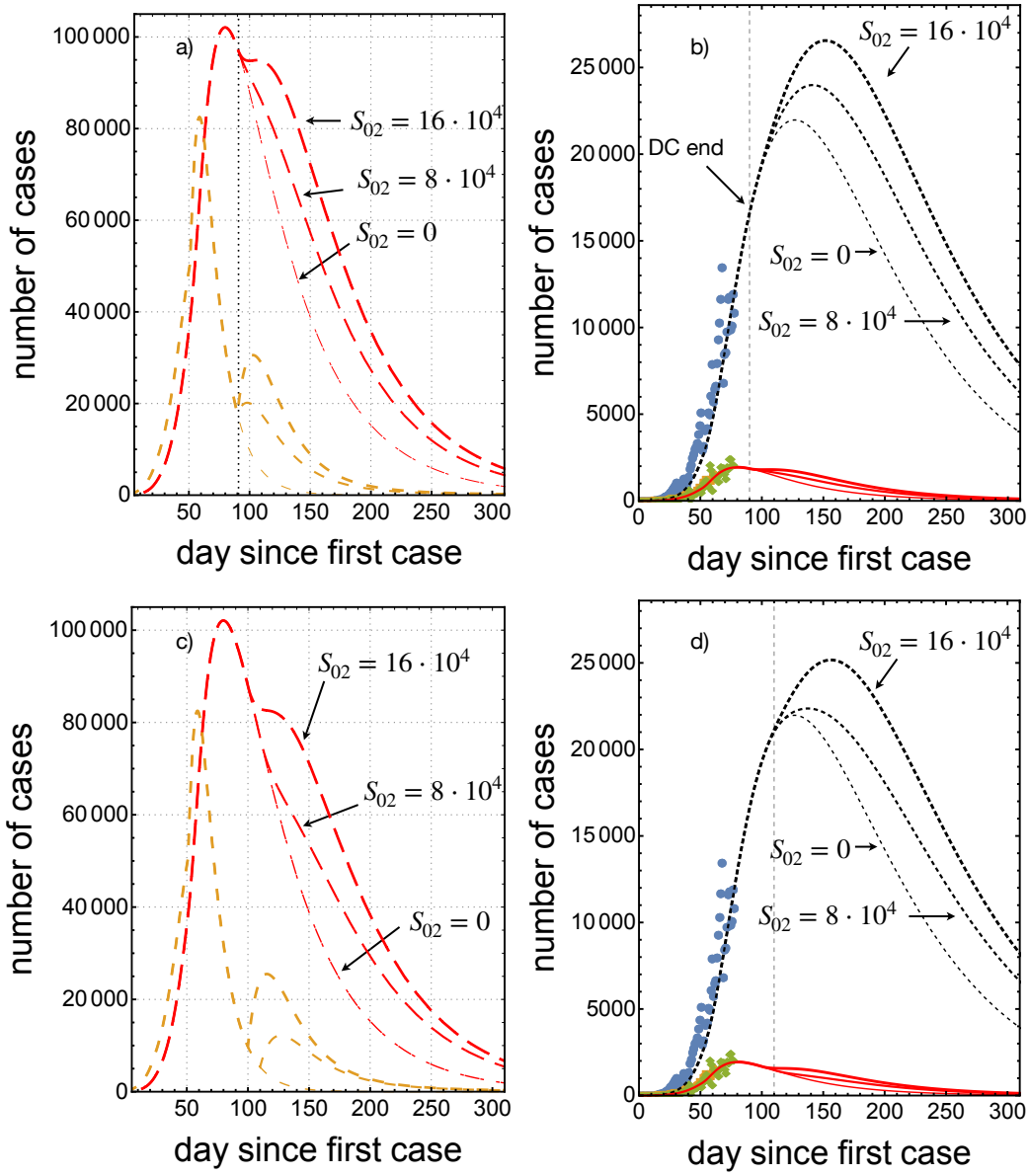

FIG. 3. Fit of the data reported by the Mexican authorities (up to July 12). a) The symbols represent infected (red circles), recovered (blue squares), and death (orange triangles) individuals, the lines the numerical solutions of Eqs. (2.12)-(2.17) for $I(t)$ (red), $R(t)$ (blue), $D(t)$ (orange), exposed $E(t)$ (magenta) and active $A(t)$ (cyan). The black dashed line is the number of confirmed cases given by Eq. (19). b) Long term projection of the fit. c) Fit of the active cases and d) of the cumulative number of daily cases $Day(t)$. The calculation of the data represented by the symbols was done using Eq. (3.2) (green diamonds squares) and Eq. (3.1) (blue circles). In the case of daily cases (orange squares).

here, the duration of the pandemic extends to 400 days. If a second possible outbreak is considered, the duration may be increased correspondingly. The cumulative number of infected individuals may also increase.

D. Model actualization

The original estimations of the susceptible population were performed using statistical information from evolution data of the European evolution of the pandemic, mainly using Italy and Spain's data, countries from where it is supposed that the SARS-CoV-2 virus was introduced in Mexico. Those data show now (11 July 2020) insufficient to estimate the number of susceptible individuals in Mexico. The origin of the underestimation is clear since managing the pandemic, the social security services, the economic and financial capabilities, and the psychological response of the populations to the epidemic is very different.

In the Mexican case, several mechanisms tremendously incremented the number of susceptible individuals since the last days of May until the first days of July. Social inattention of the distancing measures and domestic confinement, the difficulty to maintain high hygienic conditions in public spaces and transport, as well as economic pressure and general confusion on the duration and the possible extent of the pandemic in human terms, can be considered the most important.

In this section, we present an actualization of the model to the data reported until July 10. As explained before, to be reliable, we considered that the data reported by the health authorities required the simultaneous fit of the five data. The accumulated number of cases, the number of recovered individuals, the number of deaths and, emerging from these data, the number of active cases, and the number of daily new cases. The model correctly follows this tendency even by increasing the number of susceptible individuals, which passed from $S_0 \approx 400$ thousand individuals before May 19, to $S_0 \approx 850$ thousand individuals to July. We are crossing a problematic period in the pandemic evolution. The apparent premature return to the normal activities (from the pandemic evolution) makes difficult, strict monitoring of compliance with social distancing, domestic confinement, hygienic measures (like the use of face masks in public spaces), and, perhaps, restrictions of mobility among different cities. This situation's effects can be reflected in a further increase in susceptible individuals during July and the first days of August.

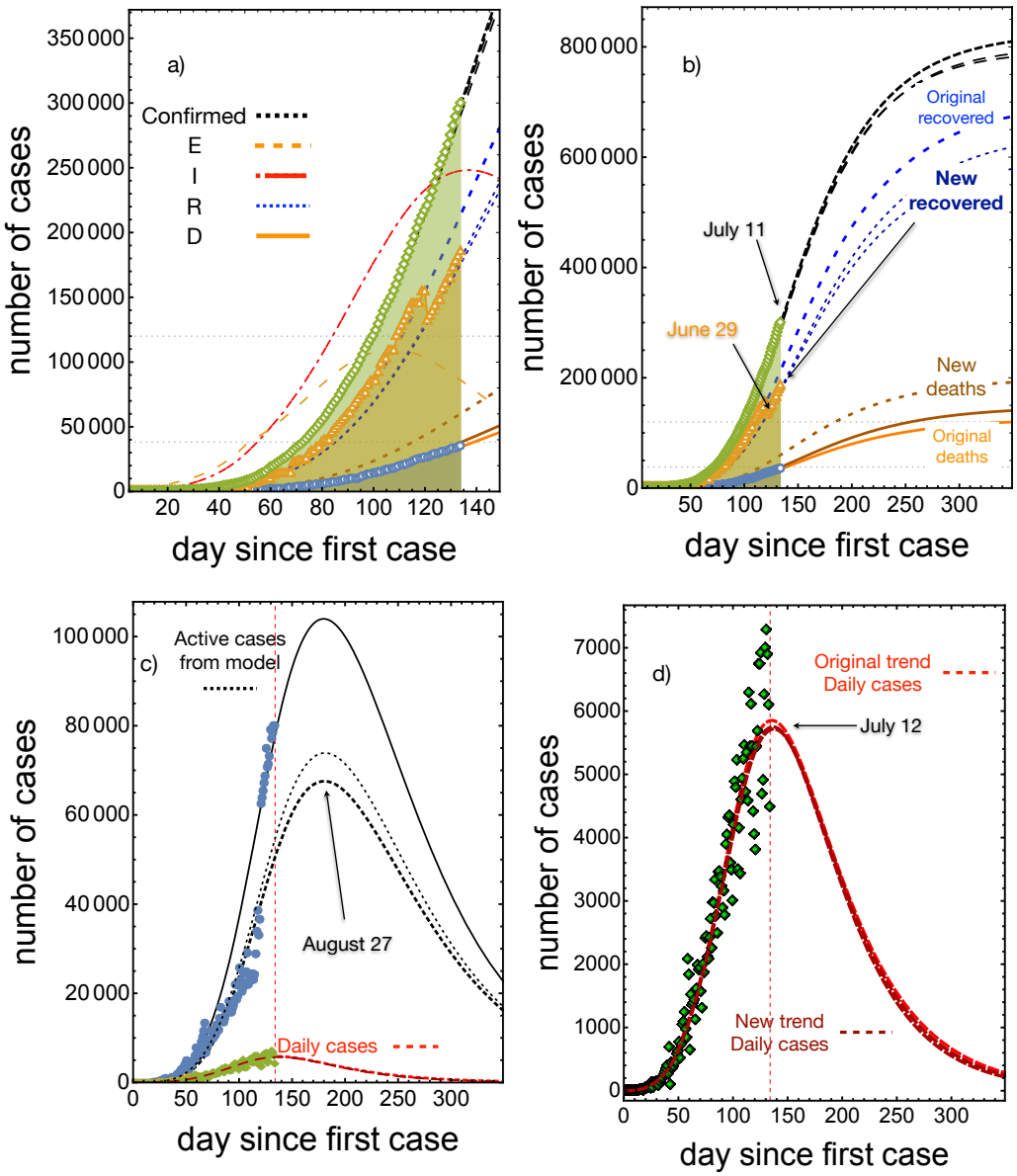

FIG. 4. Projection of the pandemic evolution with data up to July 11. a) Evolution of the pandemic after finishing domestic confinement on day 90 (May 29). Orange, dark orange and dark dashed orange lines below correspond to the number of death trends. b) Evolution of the pandemic up to day 350. c) Active and daily cases associated with a) The solid line corresponds to the new trend in recovered people warranting the fit of the active individuals. The thin dashed line in the middle is corresponds to the fit of the death number with out warranting the fit of the active individuals. d) Detail of daily cases associated with c).

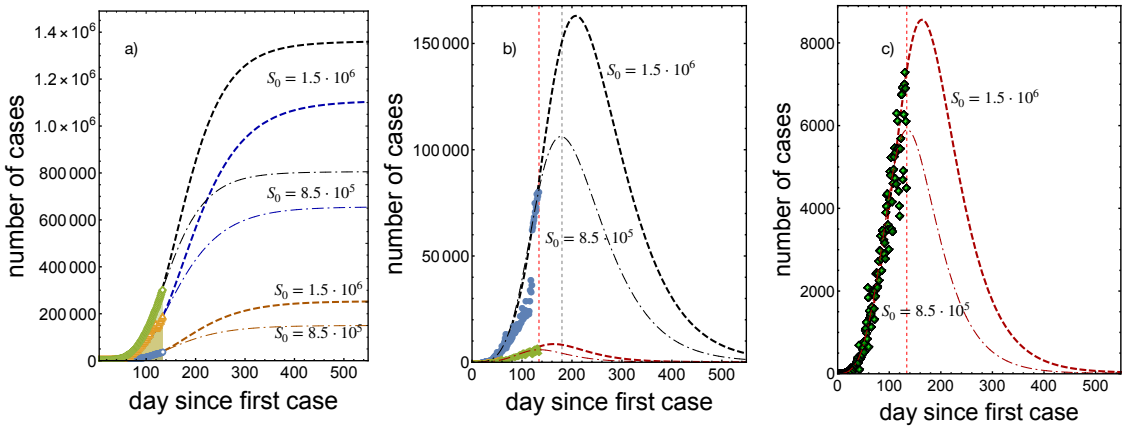

FIG. 5. Comparison of the projections of the pandemic evolution with data up to July 11 assuming two values of the total susceptible populations: $1.5 \cdot 10^6$ indicated by dashed lines and $8.5 \cdot 10^5$ indicated by dash-dotted lines. In a) the long term evolution of the accumulated number of cases (black lines), recovered (blue lines) and deaths (orange lines). b) The number of active cases (black lines) and the daily cases (red lines). c) The number of daily cases (red lines).

Concerning the new fit of data we present in this subsection, a vital issue occurred during the time going from May to July. At the end of June, the number of recovered individuals reported by the authorities decreased suddenly. On June 27, the report of recovered individuals was 153797, and on June 29, the report was 131264, a reduction of about 15% [27]. The underlying assumptions of the present model separate the fates of the infected individuals in three subpopulations: recovered, active, and death.

The number of active cases reported by the authorities is consistently is about the 70% of the number reported here (presumably because of clinical criteria to which we have no access). Because of these considerations, the restoration of the balance in the total number of individuals infected should be done by recalculating only the number of deaths, then the number of deaths increases by a factor of 1.86, see Figure 4. However, this fit is not satisfactory, since the number of active cases, as defined here, is not fitted simultaneously with the other four series of data. It is more adequate to split the difference in the number of recovered individuals between active cases and deaths in such a way that the active cases become simultaneously fitted. The resulting increase in the number of deaths is by a factor of 1.09 since, on day 133, the number of deaths reported was 35006. The model prognosis is 38200, with the assumption of 860 thousand susceptible individuals. This factor seems not

relevant at the present stage, but after 350 days, the difference becomes about 10 thousand individuals. Remarkably, the fit of the daily cases varies less than 1% with the two methods. This result suggests that the number of daily cases is not reliable enough to take dependable health policies. A more robust quantitative criterion, like the one presented here, is needed. Finally, in figure 5 we present two projections of the pandemic assuming different values of the total number of susceptible individuals. Dashed lines correspond to $S_0 = 1.5 \cdot 10^6$ whereas the dash-dotted lines to $8.5 \cdot 10^5$. Both projections satisfy the criterion of fitting the five sets of data. The fit of the daily cases for $S_0 = 1.5 \cdot 10^6$ (red dashed line) is along the highest values reported, in contrast with the fit using $8.5 \cdot 10^5$, that goes along the middle value. In the first case the maximum in the peak of daily cases shifts until day 165, that is until August 12.

IV. CONCLUSION

We have presented and employed a novel model as a conceptual tool to explore the possible fates of the COVID-19 pandemic evolution in the Mexican context. The selection and variation of control parameters in the model allow us to get insights into the system to sustain political decisions on the appropriate time for concluding domestic confinement and social distancing restrictions. The flexibility of the model allows taking into account the specific characteristics of the parameters involved, one composed by the (S, E, I, A, R, D) group and the second one by a particular population that may become susceptible after the end of the domestic confinement measure.

Our model allowed us to perform a very accurate fit of the reported data and, therefore, a reliable projection of the pandemic on the basis that the estimation on the number of susceptible individuals is realistic. We have successfully correlated the inflections of the infection, daily and active cases curves with a decrease of the infection rate after the start of the social distancing measures, and its sudden increase with the corresponding enhancement of the infection rate around the day 51 of the pandemics.

The model also allows predictions of the effect of post-social distancing and house confinement time by considering two elements: *i)* Poor hygienic conditions and *ii)* contact with an exposed individual. Based on the data published by the Mexican authorities, the results indicate that the more drastic effects take place in the number of infected individuals by an

increase in the duration of the pandemic from roughly 300 days to 400 days in the worst case considered. Additionally, the peak of the number of active cases is shifted to day 150 and increased about 23% if the date of ending social distancing is at day 90. The maximum of the curve of the active case moves towards day 160 when domestic confinement finishes at day 110. Correspondingly, the maximum number of active cases increases by about 9%. Maintaining high hygienic standards and social distancing measures is the key to successfully control the spread and outbreak of the SARS-COV-2 after domestic confinement ends. If these measures are not strictly followed, the pandemic duration can last more than a year with increases of 23-33% in the number of deaths, and 24-40% in the cumulative number of infection cases.

Ethics. This article does not present research with ethical considerations.

Data Accessibility. Supplementary material from "Possible fates of the dispersion of SARS-COV-2 in the Mexican context" submitted with DOI https://doi.org/10.5061/dryad.70rxwdbv5. See also: https://datadryad.org/stash/share/6JU8QvbDmlrDFsmapZEncfezd4FA3-iSvDiwNLVVOg4 .

Authors' Contributions. I.S.H. carried out program coding and model simulations, conceived the study, carried out the analysis of the results and drafted the manuscript; V.M.C. coordinated the study and helped draft the manuscript. All authors gave final approval for publication and agree to be held accountable for the work performed therein.

Competing Interests. We declare that we have no competing interests.

Funding. This work was supported by UNAM-DGAPA under grant IN117419.

Acknowledgements. We are grateful with Dr. Aldo Ledesma-Durán and Prof. Karo Michaelian for reading the manuscript and sharing valuable comments on the model.

[1] Dearing JA, Batterbee RW, Dikau R, Larrocque I, Oldfield F. 2006 Human-environment interactions: towards synthesis and simulation. Reg. Environ. Change **6** 115-123.

[2] Alcocer-Cuarón C, Rivera AL, Castaño VM. 2014 Hierarchical structure of biological systems, Bioengineered **2** 73-79.

[3] Motesharrei S, Rivas J, Kalnay E. 2014 Human and nature dynamics (handy): Modeling inequality and use of resources in the collapse or sustainability of societies. Ecol. Econ. **101** 90-102. (doi.org/10.1016/j.ecolecon.2014.02.014)

[4] Fu B, Li Y. 2016 Bidirectional coupling between the earth and human systems is essential for modeling sustainability. National Science Review **3** 397-398. (doi.org/10.1093/nsr/nww081)

[5] Henderson K, Loreau M. 2018 How ecological feedbacks between human population and land cover influence sustainability. PLoS Comput. Biol. **14** e1006389. (doi.org/10.1371/journal.pcbi.1006389)

[6] Fiscus DA, Fath B. 2019 *Foundations for sustainability.* Amsterdam, Elsevier.

[7] Cardinale BJ, et al. 2012 Biodiversity loss and its impact on humanity. Nature **486** 59. (doi:10.1038/nature11148)

[8] McGinnis MD, Ostrom E. 2014 Social-ecological system framework: initial changes and continuing challenges, Ecology and Society **19** 30. (dx.doi.org/10.5751/ES-06387-190230)

[9] Snacken R, Kendal AP, Haaheim LR, Wood JM. 1999 The next influenza pandemic: Lessons from hong kong, 1997, Emerg. Infect. Dis. **5** 195-203. (doi: 10.3201/eid0502.990202)

[10] Fan VY, Jamison DT, Summers LH. 2018 Pandemic risk: how large are the expected losses?, Bulletin of the World Health Organization **96** 129-134. (dx.doi.org/10.2471/BLT.17.199588)

[11] Ryan B, Coppola D, Canyon D, Brickhouse M, Swienton R. 2020 COVID-19 community stabilization and sustainability framework: An integration of the maslow hierarchy of needs and social determinants of health. Disaster Med. Public Health Prep. **21** 1-16. (doi: 10.1017/dmp.2020.109)

[12] Gómez M. 2014 Policies, complexity and the need for cooperation in epistemic inquiry for the stable use of natural resources. Environmental Science & Policy **37** 91-100.

[13] Aguado C, Castaño VM. 2020 Translational knowledge map of COVID-19. arXiv:2003.10434. (https://arxiv.org/abs/2003.10434)

[14] Daughton AR, Generous N, Priedhorsky R, Deshpande A. 2017 An approach to and web-based tool for infectious disease outbreak intervention analysis. Scientific Reports **7** 46076. (doi: 10.1038/srep46076)

[15] Acuña-Zegarra MA, Cibrian MS, Velasco-Hernández JX. 2020 Modeling behavioral change and covid-19 containment in Mexico: A trade-off between lockdown and compliance. Math. Biosci. in press. (doi: 10.1016/j.mbs.2020.108370)

[16] Ferreti L, et al. 2020 Quantifying sars-cov-2 transmission suggests epidemic control with digital contact tracing. Science **368** 6491. (doi:10.1126/science.abb6936)

[17] Nokes DJ, Anderson RM 1988 The use of mathematical models in the epidemiological study of infectious diseases and in the design of mass immunization programmes. Epidemiol. Infect. **101** 1-20. (doi: 10.1017/s0950268800029186)

[18] Wonham MJ, de Camino-Beck T, Lewis MA. 2004 An epidemiological model for west nile virus: invasion analysis and control applications, Proc. Biol. Sci. **271** 501-507. (doi: 10.1098/rspb.2003.2608)

[19] Adams B, Boots M. 2010 How important is vertical transmission in mosquitoes for the persistence of dengue? insights from a mathematical model. Epidemics **2** 1-10. (doi: 10.1016/j.epidem.2010.01.001)

[20] Onyejekwe OO, Tigabie A, Ambachew B, Alemu A. 2019 Application of optimal control to the epidemiology of dengue fever transmission. J. App. Math. Phys. **7** 148-165. (doi: 10.4236/jamp.2019.71013)

[21] Njeuhmeli E, et al. 2019 Using mathematical modeling to inform health policy: A case study from voluntary medical male circumcision scale-up in eastern and southern Africa and proposed framework for success. PloS ONE **14** e0213605. (doi.org/10.1371/journal.pone.0213605)

[22] Dever GA. 1976 An epidemiological model for health policy analysis. Social Indicators Research **2** 453-466. (doi: 10.1007/BF00303847)

[23] Escudero FA, Goldhaber-Fiebert J. 2020 *CIDE y Stanford desarrollan modelo matemático de proyecciones sobre COVID19.* See https:/www.cide.edu//saladeprensa/cide-y-stanford-desarrollan-modelo-matematico-de-proyecciones-sobre-covid-19/(2020).

[24] Zhou F. et al. 2020 Clinical course and risk factors for mortality of adult inpatients with COVID-19 in Wuhan, China: a retrospective cohort study. Lancet **395** 1054-1062. (doi: 10.1016/S0140-6736(20)30566-3)

[25] Heiden M, Buchholz U. 2020 Modellierung von Beispielszenarien der SARS-CoV-2-Epedemie 2020 in Deutschland. Robert Koch Institut, Germany. See https://doi.org/10.25646/6571.2

[26] Phua J. 2020 Intensive care management of coronavirus disease 2019 (COVID-19): challenges and recommendations. Lancet Respir. Med. **8** 506-517. (doi: 10.1016/S2213-2600(20)30161-2)

[27] Dirección General de Epidemiología. 2020 *Información General. Coronavirus Gob MX*. See https://coronavirus.gob.mx/datos/

[28] Instituto Nacional de Geografía y Estadística. 2008 *Distribucion de la poblacion mexicana y su economia sectorial*. See https://www.inegi.org.mx/inegi/spc/doc/INTERNET/1-GEOGRAFIADEMEXICO/MANUAL DISTRIB POB MEX VS ENERO 29 2008.pdf See http://cuentame.inegi.org.mx/poblacion/rur urb.aspx?tema=P

[29] Santamaria-Holek I, Castaño VM. 2020 *Supplementary material from "Possible fates of the dispersion of SARS-COV-2 in the Mexican context"*. See https://datadryad.org/stash/share/6JU8QvbDmlrDFsmapZEncfezd4FA3-iSvDiwNLVVOg4. See also https://doi.org/10.5061/dryad.70rxwdbv5.

[30] J. A. Dearing, R. W. Batterbee, R. Dikau, I. Larrocque, F. Oldfield, Human-environment interactions: towards synthesis and simulation, Reg. Environ. Change 6 (2006) 115–123.

[31] C. Alcocer-Cuarón, A. L. Rivera, V. M. Castano, Hierarchical structure of biological systems, Bioengineered 2 (2014) 73–79.

[32] S. Motesharrei, J. Rivas, E. Kalnay, Human and nature dynamics (handy): Modeling inequality and use of resources in the collapse or sustainability of societies, Ecological Economics 101 (2014) 90–102.

[33] B. Fu, Y. Li, Bidirectional coupling between the earth and human systems is essential for modeling sustainability, National Science Review 3 (4) (2016) 397–398.

[34] K. Henderson, M. Loreau, How ecological feedbacks between human population and land cover influence sustainability, PLoS computational biology 14 (8) (2018) e1006389.

[35] D. A. Fiscus, B. Fath, Foundations for sustainability, Elsevier, Amsterdam., 2019.

[36] B. J. Cardinale, J. E. Duffy, A. Gonzalez, D. U. Hooper, C. Perrings, P. Venail, A. Narwani, G. M. Mace, D. Tilman, D. A. Wardle, et al., Biodiversity loss and its impact on humanity, Nature 486 (7401) (2012) 59.

[37] M. D. McGinnis, E. Ostrom, Social-ecological system framework: initial changes and continuing challenges, Ecology and Society 19 (2014) 30.

[38] R. Snacken, A. P. Kendal, L. R. Haaheim, J. M. Wood, The next influenza pandemic: Lessons from hong kong, 1997, Emerg Infect Dis. 5 (1999) 195–203.

[39] V. Y. Fan, D. T. Jamison, L. H. Summers, Pandemic risk: how large are the expected losses?, Bulletin of the World Health Organization 96 (2018) 129–134.

[40] J. Diamond, Collapse: How societies choose to fail or succeed, Penguin, 2005.

[41] B. Ryan, D. Coppola, D. Canyon, M. . Brickhouse, R. Swienton, Covid-19 community stabilization and sustainability framework: An integration of the maslow hierarchy of needs and social determinants of health, Disaster Med. Public Health Prep. 21 (2020) 1–16.

[42] M. Gómez, Policies, complexity and the need for cooperation in epistemic inquiry for the stable use of natural resources, Environmental, Science & Policy 37 (2014) 91–100.

[43] C. Aguado, V. M. Castano, Translational knowledge map of covid-19, arXiv:2003,10434 (2020) 1–16.

[44] A. R. Daughton, N. Generous, R. Priedhorsky, A. Deshpande, An approach to and web-based tool for infectious disease outbreak intervention analysis, Scientific Reports 7 (2017) 46076.

[45] M. A. Acuna-Zegarra, M. S. Cibrian, J. X. Velasco-Hernández, Modeling behavioral change and covid-19 containment in mexico: A trade-off between lockdown and compliance, Mathematical Biosciences, in press`doi:10.1016/j.mbs.2020.108370`.

[46] L. F. et al., Quantifying sars-cov-2 transmission suggests epidemic control with digital contact tracing, Science`doi:10.1126/science.abb6936`.

[47] D. J. Nokes, R. M. Anderson, The use of mathematical models in the epidemiological study of infectious diseases and in the design of mass immunization programmes., Epidemiol Infect. 101 (1988) 1–20.

[48] M. J. Wonham, T. de Camino-Beck, M. A. Lewis, An epidemiological model for west nile virus: invasion analysis and control applications, Proceedings of the Royal Society of London. Series B: Biological Sciences 271 (1538) (2004) 501–507.

[49] B. Adams, M. Boots, How important is vertical transmission in mosquitoes for the persistence of dengue? insights from a mathematical model, Epidemics 2 (2010) 1–10.

[50] O. O. Onyejekwe, A. Tigabie, B. Ambachew, A. Alemu, Application of optimal control to the epidemiology of dengue fever transmission, Journal of Applied Mathematics and Physics 7 (2019) 148–165.

[51] E. Njeuhmeli, M. Schnure, A. Vazzano, E. Gold, P. Stegman, K. Kripke, M. Tchuenche, L. Bollinger, S. Forsythe, C. Hankins, Using mathematical modeling to inform health policy: A case study from voluntary medical male circumcision scale-up in eastern and southern africa and proposed framework for success, PloS one 14 (3) (2019) e0213605.

[52] G. A. Dever, An epidemiological model for health policy analysis, Social indicators research 2 (4) (1976) 453–466.

[53] F. A. Escudero, J. Goldhaber-Fiebert, Cide y stanford desarrollan modelo matemático de proyecciones sobre covid19, Sala de prensa CIDE. https/www.cide.edu//saladeprensa/cide-y-stanford-desarrollan-modelo-matematico-de-proyecciones-sobre-covid-19/(2020).